

An Unusual Structure of an As-cast 30% Cr Alloy White Iron

A. WIENGMOON, T. CHAIRUANGSRI¹⁾ and J. T. H. PEARCE²⁾

Department of Physics, Faculty of Science, Chiang Mai University, 50200, Thailand. E-mail: amporn_ka@hotmail.com

1) Department of Industrial Chemistry, Faculty of Science, Chiang Mai University, 50200, Thailand.

2) National Metal and Materials Technology Center, Bangkok, 10400, Thailand.

(Received on March 22, 2005; accepted on July 17, 2005)

An unusual microstructure of an as-cast 30 wt% Cr and 2.26 wt% C iron has been examined by optical microscopy (OM), scanning electron microscopy (SEM) and transmission electron microscopy (TEM). It was found that the microstructure varied with positions in the cast bar. In the upper part of the cast bar where the cooling rate was faster, the matrix was essentially austenite with some patches of ferrite-plus-precipitated carbides as dendritic regions. Whereas, the central and the lower parts of the cast bar where cooling rates were slower, there was less austenite with greater amount of ferritic zones. The microstructure of core regions at the centre of the dendritic ferrite-plus-precipitated carbides zones contained interconnected carbides that are believed to be the product of a peritectic reaction. TEM examination confirmed that these peritectic carbides were M_7C_3 type. Bainite and martensite were also observed in the transition zones close to the ferrite-plus-precipitated carbides zones. These were believed to result from solid-state decomposition of the dendritic austenite in the later stage of cooling.

KEY WORDS: high chromium cast iron; microstructure; electron microscopy; peritectic reaction.

1. Introduction

Due to the presence of hard eutectic carbides in their microstructures, high chromium cast irons are suitable for abrasion resistant applications in industries such as cement manufacture and mineral processing.^{1–6)} These irons are almost always designed to have hypoeutectic compositions, containing 11–30 wt% Cr and 2–3.3 wt% C, to avoid the formation of any primary carbides that would impair toughness. Depending on carbon and chromium levels, the hypoeutectic irons contain between 15–35% by volume of eutectic carbides. They can be used with austenitic matrices, which work harden in some service situations, or with hardened and tempered martensitic matrices.^{5,6)}

The alloys containing 28–30 wt% Cr and 2.0–2.7 wt% C have been specially developed to resist the combined effects of abrasion and corrosion in wet wear applications such as slurry pumping.^{6,7)} The as-cast microstructure of these 28–30 wt% Cr irons consists of primary austenite dendrites with eutectic austenite (partially transformed to martensite) and eutectic M_7C_3 type carbide in the interdendritic regions.^{8–12)} The extent to which primary and eutectic austenite remains untransformed on cooling depends upon its composition and the cooling rate in the mould from solidification down to ambient temperatures. Austenite retention is favoured by a high Cr:C ratio, by the presence of alloy additions such as Mo, Ni, Cu, *etc.* and by faster cooling (*i.e.* smaller cast section sizes).

Chromium acts as a ferrite promoter expanding the primary ferrite phase field and contracting the primary austenite phase field. Hence at the 28–30% Cr level if the Cr:C ratio is high then primary dendrites of δ ferrite, not austenite,

are formed and an iron with 2 wt% C and 30 wt% Cr will therefore have a microstructure consisting of ferrite and eutectic carbides.¹³⁾ At elevated temperatures, Cr increases the solubility of C in ferrite such that as-cast ferrite at ambient temperature can be supersaturated with C and will precipitate carbides if heat treated.¹⁴⁾ Free ferrite can also be formed at lower Cr levels if the silicon level is high *e.g.* at 20wt%Cr–2.6wt%C in an iron with 2.6% Si, however its mechanism of formation is not fully understood.¹³⁾ Ferrite is normally undesirable in abrasion resistant irons since it is softer than austenite and does not work harden significantly during wear service.^{15,16)} For 30 wt% Cr irons with 2–2.5 wt% C levels, it is difficult for foundries to predict whether the primary dendrites will be austenite or ferrite since there is some uncertainty over the equilibrium positions of the $L + \delta \rightarrow \gamma$ peritectic line and the U_1 peritectic point,^{17,18)} and over the effects of cooling rate during solidification on these reactions.

This paper examines unusual microstructural and crystallographic features of an as-cast 2.3wt%C–30wt%Cr iron with normal silicon and manganese levels, and without any added Mo, Cu or Ni.

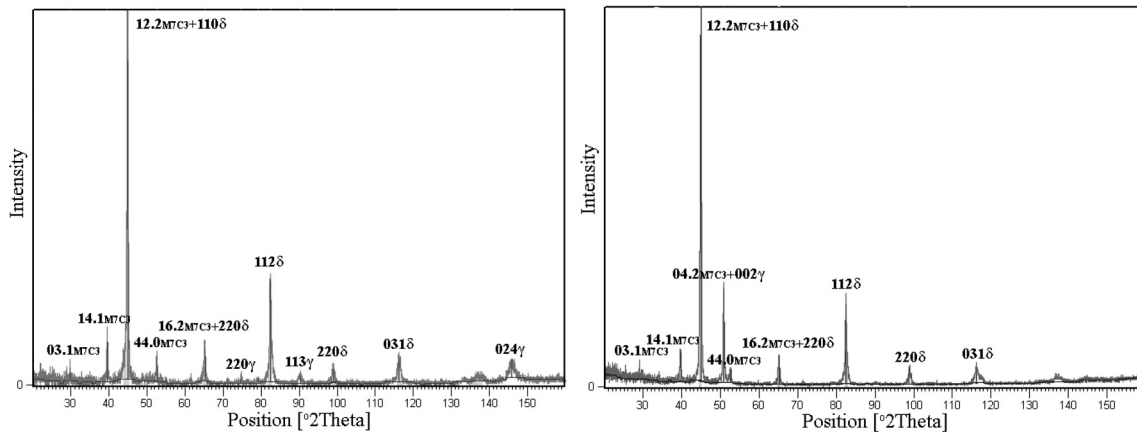
2. Materials and Methods

2.1. Materials Preparation

The chemical composition of the alloy used is given in **Table 1**. The alloy was prepared by induction melting of a charge of low Si pig iron and ferroalloys. The melt was cast into CO_2 -silicate moulds to provide cylindrical bars 300 mm long by 25 mm in diameter at a pouring temperature of 1500°C. After removal of feeder heads, each bar

Table 1. Chemical composition of alloy.

Alloy	Composition (wt%)									
	C	Cr	Si	Mn	S	P	Ni	Cu	Mo	Al
A	2.26	29.98	0.52	0.30	0.013	0.025	0.30	0.02	0.08	0.009

**Fig. 1.** As-cast 30%Cr–2.3%C iron: X-ray diffraction traces from (a) upper parts and (b) lower part of a test bar.

was sectioned transversely to give specimens with an approximate thickness of 15 mm.

2.2. Sample Preparation for Microstructural Investigation

Metallographic specimens for optical microscopy (OM) and scanning electron microscopy (SEM) were mounted in resin, ground on silicon carbide papers to 1200 grit and then polished to 1 μm diamond finish. The etchants used were (1) 50 mL of HCl and 10 g of $\text{Na}_2\text{S}_2\text{O}_5$ in 100 mL distilled water, to reveal the ferritic and austenitic microstructure, and (2) 10% HCl in methanol for 6 h for deep etching to examine the morphology of carbides. The microstructures were observed using a JEOL JSM-5410LV scanning electron microscope. Chemical microanalysis was performed using an Oxford Instruments ATW2 X-ray Spectrometer. The SEM was operated at 20 kV using a working distance of 17 mm from the objective lens.

Thin foils for transmission electron microscopy (TEM) were prepared by sectioning specimens, perpendicular to the axis of the as-cast cylindrical rod, with a cubic boron nitride saw to obtain slices with a thickness of about 200 μm . These were then ground manually on silicon carbide papers (down to 1200 grit) to reduce their thickness to about 80 μm . Discs, 3 mm in diameter, were then punched out and thinned with a Struers, Tenupol-3 twin-jet electropolisher operated at 15 V and approximately 20 μA , using a solution containing 10% perchloric acid and 30% of 2-butoxy-ethanol in absolute ethanol maintained at -15°C . The thin samples were argon-ion-beam-thinned using a Gatan model 600 DIF Duo Mill ion beam thinner for final stage thinning. They were then examined using a JEOL JEM-2010 scanning-transmission electron microscope, operated at 200 kV.

2.3. Hardness Measurement

The specimens prepared for SEM were also used for hardness determination. A Galileo microhardness tester was used to measure the Vickers microhardness of the

dendritic regions on etched specimens using 100 gf load (0.1 kgf) and 15 s indenting time. The mean values are based on ten different indentations.

2.4. X-ray Diffraction (XRD) Analysis

Samples with 20 mm square faces for XRD were prepared in the same way as the samples for OM and SEM but without etching. The phases present in the alloy were then determined using a Philips X'pert diffractometer with a $\text{Cu K}\alpha$ X-ray source set to cover a 2θ range of 10–120 degrees and to record data at 0.04 degrees steps at a speed of 0.004 degrees/min.

3. Results and Discussion

3.1. General Microstructure and XRD

Although, alloy A has previously¹⁹⁾ been described as an austenitic iron, its microstructure was found to vary with position in each as-cast test bar depending on the cooling rate. During casting, the bars were bottom filled such that the lower part of each bar would have cooled at a slower rate than the upper part. The faster cooling at the upper parts of each bar has encouraged the formation and retention of an austenite matrix with some patches of ferrite containing precipitated carbides. The central portion of each bar contained less austenite and in the lower region, next to the ingate, the matrix was essentially fully ferritic with precipitated carbides. XRD results, seen in **Fig. 1**, confirmed that the upper and central regions of the as-cast bar consist of austenite, ferrite and M_7C_3 carbides. These general microstructural features are illustrated in **Fig. 2**, which gives low magnification optical views of a section from an upper region of a cast test bar. Areas of dendritic austenite and eutectic carbides (A) and darker etching dendritic zones of ferrite containing precipitated carbides (B) can be clearly distinguished. In addition, there is an unusual microstructural feature (marked C) at the central area of each zone of dendritic ferrite. This appears to consist of a mixture of eu-



Fig. 2. (a) General microstructure from upper region of test bar. Areas of dendritic austenite plus eutectic M_7C_3 carbides are indicated as (A) whilst the dendritic matrix of ferrite and carbide precipitates (darker etching) are marked (B). (b) This view shows an apparent dendrite free zone at the core of a ferrite area, marked (C). Optical view: Etchant is 50 mL of HCl and 10 g of $Na_2S_2O_3$ in 100 mL distilled water.

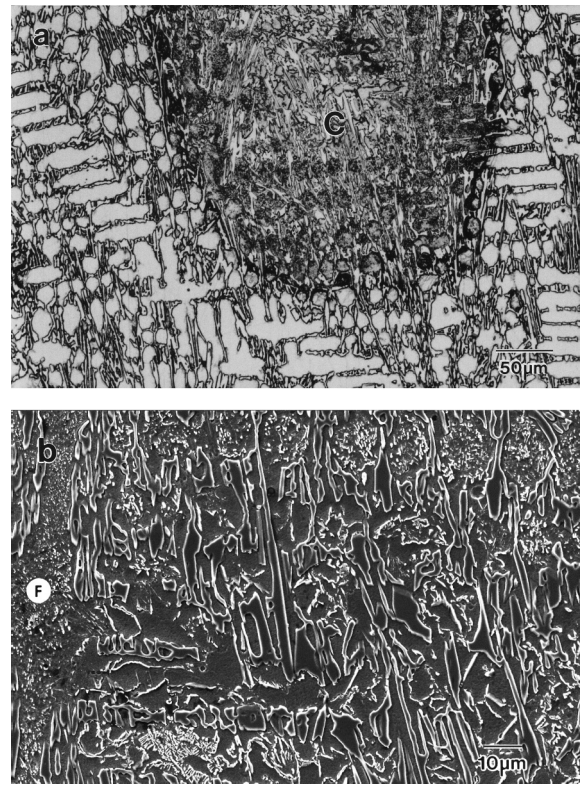


Fig. 3. (a) Optical view showing dendritic austenite regions free of secondary carbide precipitation and darker regions where precipitation has allowed transformation of these dendrites to ferrite. The primary dendrite structure is not clearly defined at the centre of the ferritic zone (C). (b) Secondary electron image (SEI) of core region showing rod-like eutectic M_7C_3 carbides and other forms of carbides. Primary dendrite arms, now consisting of ferrite plus fine secondary carbides, are indicated by F.

tectic and other carbides in a ferritic matrix where the original primary dendrite form cannot be clearly distinguished and where the precipitation density of the secondary carbides is much less than in the clearly defined dendritic regions. These differences are illustrated by the optical and SEM versions in **Fig. 3**.

Transformation of the dendritic austenite to martensite was significant in the transition zones between the austenite dendrites and the ferrite-plus-precipitated-carbides dendritic regions as seen in **Fig. 4**. There must be compositional differences *e.g.* reduction in Cr and C levels in the growing dendrite arms during solidification that reduce the stability of the austenite during subsequent solid state cooling.

3.2. Microhardness of the Dendritic Matrix

The results given in **Table 2** show that, as expected, the microhardness of the austenite dendrites was higher than for the ferritic zones since the austenite dendrites have a higher level of carbon solubility. The microhardness of the core regions (marked "C" in **Fig. 2(b)**) varied from 315–375 Hv while that of the surrounding dendritic ferrite varied from 364 to 395 Hv. Due to the presence of secondary carbide precipitation, these hardness levels are higher than 290–310 Hv recorded previously for precipitate-free ferrite in a 36%Cr–2.13%C iron.³⁾ The microhardness measurements in the austenite dendrites varied from 456 to 592 Hv compared to values of 374–447 Hv for austenite dendrites in an as-cast 30.6%Cr–2.44%C iron.^{3,16)} The

higher hardness was believed to be due to a higher tendency of the austenite in iron A to partially transform to martensite.

3.3. Microstructure and Solidification Sequences in 30 % Cr Iron

The deep-etched microstructure of a core region at the centre of a dendritic ferrite plus precipitated carbides zone is illustrated in **Fig. 5**. Patches of interconnected carbide, later identified as M_7C_3 , can be seen in relation to the surrounding rods of eutectic M_7C_3 which are much coarser. These finer carbides are believed to be the product of a peritectic reaction since they exhibit a quite different morphology to the eutectic M_7C_3 and to the secondary carbides that have precipitated and grown as a network in the dendritic regions. This network is also revealed by deep-etching as seen in **Figs. 6** and **7**. The cubic rod-like nature, apparent in **Fig. 7** suggests that these precipitated carbides are $M_{23}C_6$ as in the previous work on 30% Cr irons.^{8,12,19–20)} Also visible in **Fig. 7** are very thin lath-like precipitates which are believed to be bainitic carbides, but further work is needed to investigate these and the nature of austenite transformation behavior in this alloy.

Possible solidification sequences of alloy A are now considered in relation to published phase equilibria for the Fe–Cr–C ternary system, where the two most accepted studies are by Jackson¹⁷⁾ and by Thorpe and Chicco.¹⁸⁾

Table 2. Vickers microhardness in dendritic austenite and ferrite regions of an as-cast 30%Cr–2.3%C iron.

Area	Hardness (Hv (100gf/15s))										
	1	2	3	4	5	6	7	8	9	10	Mean
Core (ferrite + M_7C_3 carbide)	354	355	375	369	315	332	362	347	348	352	351
Dendritic ferrite and precipitate	379	395	391	390	392	380	383	374	364	378	383
Austenite dendrite	456	590	592	552	480	460	481	521	544	524	520

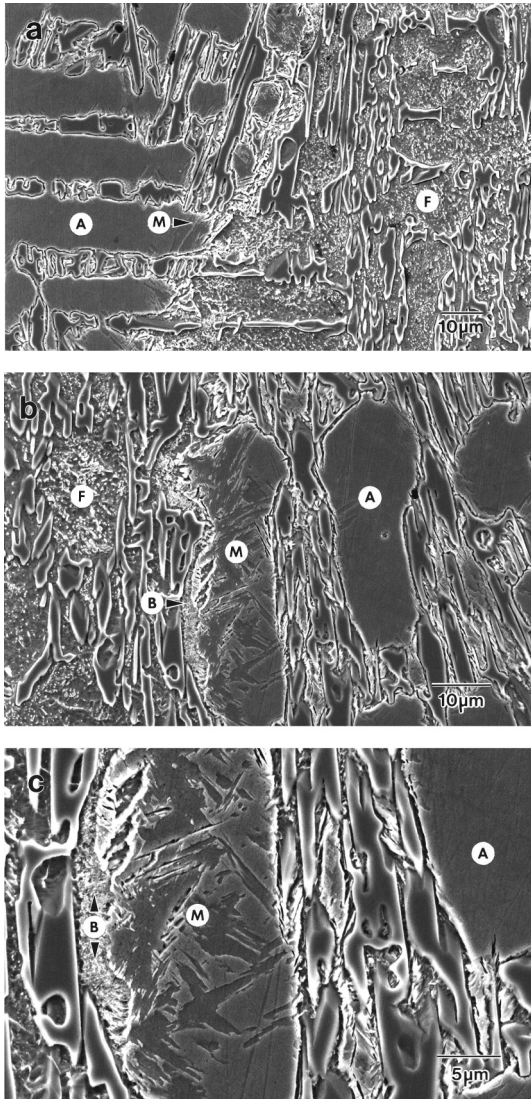


Fig. 4. (a) SEI shows austenite dendrite arms (A) which have transformed to ferrite plus carbides (F) and to martensite (M). Views (b) and (c) show increasing amounts of transformation to martensite and possibly bainite, indicated by B, in adjacent dendrite arms, compared to the area of ferrite plus carbides (F).

The liquidus surfaces from each of these studies are given in **Fig. 8**. In both versions, the positions of the $\gamma\text{Fe}-M_7C_3$ eutectic trough are in fairly close agreement, but the positions of the peritectic points U_1 and U_2 are notably different. The positions of the quasi-peritectic point U_1 and the peritectic line P_1U_1 for the reaction $L + \text{bcc } \delta\text{Fe} \rightleftharpoons \text{fcc } \gamma\text{Fe}$ are relevant to the present study.

Later work by Chicco and Thorpe²¹⁾ has confirmed the positions of U_1 and U_2 and has restated the equilibrium reactions as:

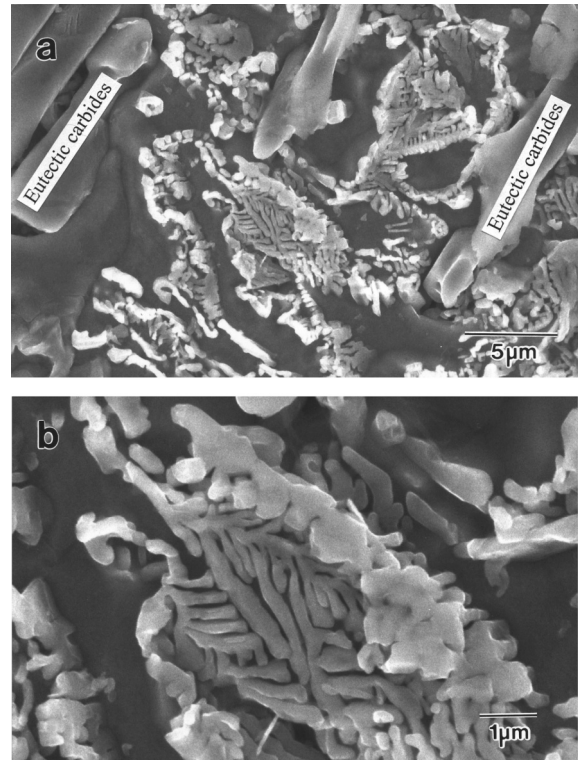


Fig. 5. SEI view of a core region at the centre of ferritic zones after deep etching. (a) Isolated patches of peritectic M_7C_3 can be seen in comparison with coarser eutectic M_7C_3 carbide. (b) Higher magnification at an area of M_7C_3 carbide believed to be formed by a peritectic reaction.

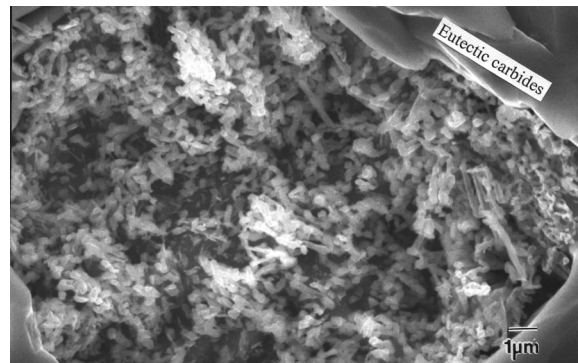
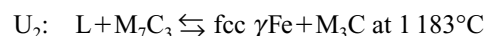
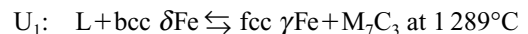


Fig. 6. SEI shows the nature of carbide precipitates in the dendritic ferrite matrix regions. Previous works and the cubic rod morphology suggest that these are $M_{23}C_6$. Etchant: 10% HCl in methanol, deep-etching.



Evidence has also been considered²²⁾ for the U_1 reaction to

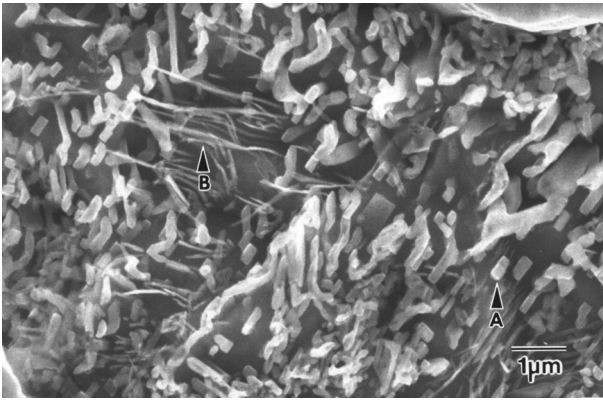


Fig. 7. Cubic morphology of fine precipitated carbides believed to be $M_{23}C_6$ (A). Also visible are very fine lath-like precipitates which could be carbides produced *via* a bainite reaction, denoted by B.

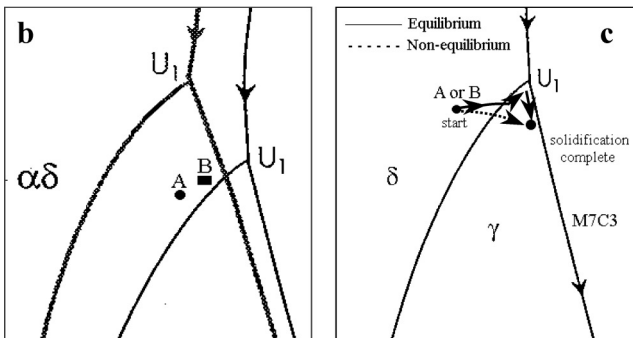
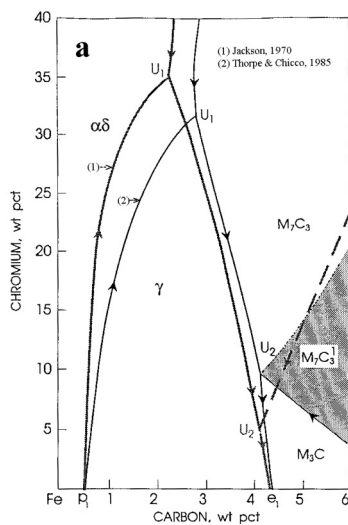


Fig. 8. (a) Iron rich corner of metastable C–Cr–Fe liquidus surface. Comparison of the position of the liquidus surface and invariant points between previous works.^{17,18} (b) Comparison of the position of the composition of Alloy A, 29.98%Cr–2.26%C iron (denoted by A) and Alloy B, 30.6%Cr–2.44%C iron (denoted by B). (c) A schematic drawing of the solidification sequence of Alloy A or B are indicated by the arrows.

produce $M_{23}C_6$, instead of M_7C_3 , at the lower equilibrium reaction temperature of 1275°C. The composition of alloy A (29.98Cr, 2.26C) in this study and that of a previously studied alloy B (30.6Cr, 2.44C)^{16,20} are also plotted in Fig. 8. The Jackson system predicts that both A and B would solidify as primary austenite followed by a eutectic reaction to produce austenite plus M_7C_3 carbide. However, from the

Thorpe and Chicco system, under equilibrium conditions both irons are in the primary ferrite phase field with the composition of iron B lying much closer than that of alloy A to the P_1U_1 peritectic line.

Hence, both irons would be expected to begin solidification as primary δ ferrite which, when the liquid metal composition reaches the P_1U_1 line, then undergoes a peritectic reaction to produce austenite. This peritectic reaction continues on further cooling down to the U_1 point. Under equilibrium conditions the liquid and remaining δ ferrite would then react at U_1 to produce the quasi-peritectic mixture of γ austenite and M_7C_3 carbide, with solidification finally being completed by any remaining liquid transforming to a eutectic mixture of γ austenite and M_7C_3 carbides. This sequence is indicated schematically by the arrows in Fig. 8(c).

Previous works^{16,20} have shown that the as-cast microstructure of alloy B, when cast as small coupons (15×30×55 mm in size) consisted of primary austenite dendrites and eutectic of austenite (partially transformed to martensite) and M_7C_3 carbide. Much of the discussion and uncertainty in the literature^{17,18,21,22} regarding the equilibrium positions and nature of the peritectic reactions at U_1 and U_2 has centred on the effects of cooling rate. As in simple binary systems, a peritectic reaction can be suppressed by fast cooling which limits the time for diffusion through the barrier product phase. In alloy B, there was no evidence in the microstructure of the U_1 peritectic reaction. The cooling rate in the small test coupons did not allow this reaction to occur and liquid metal under-cooled to follow a solidification path similar to that of a lower Cr alloy (*e.g.* 28%) directly down to the U_1U_2 eutectic, as indicated in Fig. 8(c). Assuming that δ ferrite was nucleated, the $L + \delta Fe \rightleftharpoons \gamma Fe$ reaction would be expected to go to completion due to the high rate of diffusion of interstitial C atoms. However, it may be that nucleation of δ -ferrite dendrites is suppressed and that in their place austenite dendrites are nucleated directly.

In high Cr irons at the 25–30% Cr level, M_7C_3 does not normally precipitate in the solid state, the usual precipitate is $M_{23}C_6$. M_7C_3 only precipitates in 15–20% Cr irons. For alloy A, due to its lower C level and its slower rate of cooling, when cast as test bars (300 mm×25 mm in diameter), it is believed that the quasi-peritectic at U_1 has not been completely suppressed, and that this reaction has resulted in the unusual form of M_7C_3 shown in Fig. 5. As stated earlier, TEM examination confirmed that this suspected peritectic carbide was M_7C_3 . **Figure 9** shows a bright field TEM micrograph of carbides within a ferrite matrix and the corresponding selected area diffraction pattern taken from a precipitate and the matrix. The diffraction pattern confirms that precipitate is M_7C_3 carbide and the matrix is ferrite. There is no rational orientation relationship between this carbide and the matrix.

During solidification, some δ -Fe has taken part in the U_1 peritectic reaction to produce austenite and M_7C_3 at a number of centres as shown schematically in **Figs. 10(a)** and **10(b)**, but in each case has been impinged by growing austenite dendrites. These austenite dendrites would be expected to result from the P_1U_1 peritectic reaction between initial primary ferrite dendrites and liquid but, because of non-equilibrium effects, austenite dendrites could have nu-

cleated directly from the liquid. Solidification of the remaining liquid is completed by the formation of the eutectic mixture of austenite and M_7C_3 carbide (Fig. 10(c)). During their phase equilibria studies,^{18,21)} Thorpe and Chicco noted that, for an alloy containing 29 wt% Cr and 1.7 wt% C, the $L + \delta Fe \rightleftharpoons \gamma Fe$ reaction appeared to go almost to completion and they showed microstructural evidence of this reaction. However, similar microstructural features were not seen in the austenite dendritic microstructures of alloy A or B. Hence, it is believed that the austenite dendrites grew directly from the liquid having been initially nucleated by δ ferrite which was later completely consumed. In some areas, δ ferrite was formed at temperatures just above that of the U_1 reaction and this ferrite took part in the quasi-peritectic U_1 reaction. It is recognized that the liquid path in a primary solidification phase field cannot be accurately predicted from a ternary phase diagram.¹⁸⁾ A detailed differential thermal analysis (DTA) study is needed to produce a better understanding of the solidification sequences in these alloys. The schematic diagrams in Fig. 10 are intended to provide only a tentative explanation of the complex solidification pattern of this type of iron.

After full solidification, the fcc- γFe went further through solid state transformation, starting at the peritectic zone due probably to the lower Cr content, to be bcc-Fe plus fine secondary carbides, bainite and martensite, the volume fraction of which is depending on the cooling rate. In the upper zone of the cast bar where the cooling rate was faster, higher number density of bcc-Fe patches nucleated and a smaller volume of fcc- γFe partly transformed to bcc-Fe plus carbides, followed by bainite and martensite reactions (Fig. 11(a)). On the other hand, at the lower zone of the cast bar where the cooling rate was slower, a lower number density of bcc-Fe patches nucleated but a greater volume of fcc- γFe extensively transformed to bcc-Fe plus carbides with less bainite and martensite reactions (Figs. 11(b) and 11(c)). In this study, the total volume fraction of the ferritic regions varies from about 31% in the upper part to 63% in the central part and 81% in the lower part of the cast bar. During this solid state transformation, the eutectic M_7C_3 carbides were undisturbed and hence appeared as iso-structural as can be seen in Fig. 2. This solid state transformation cannot be explained by using the phase equilibria provided by Jackson¹⁷⁾ and Thorpe and Chicco.¹⁸⁾ Isolethal sections of the complicated ternary Fe-Cr-C system at particular compositions are required and further work on relation of phase equilibria with solidification sequence is needed to support the mechanism proposed above.

4. Concluding Remarks

When considering the solidification of commercial grades of High Chromium Iron, foundries still tend to refer the earlier liquidus surface of Jackson or to the simplified partial quasi-binary phase diagrams plotted by Arnold and Sare.²³⁾ This could be misleading for irons at the 30% Cr level especially when the carbon level is below 2.5%. It is difficult to predict the primary dendrite structure and subsequent solidification path of the 30% Cr irons with composition close to the peritectic (P_1U_1) line. The presence of area of unexpected peritectic M_7C_3 and dendritic regions of ferrite plus precipitated carbides instead of austenite may contribute to the sometimes unpredictable variation in wear performance of 30% Cr irons in slurry pump applications.

If the carbon content of 30% Cr iron is too low, the composition will lie in the primary ferrite phase field. In such

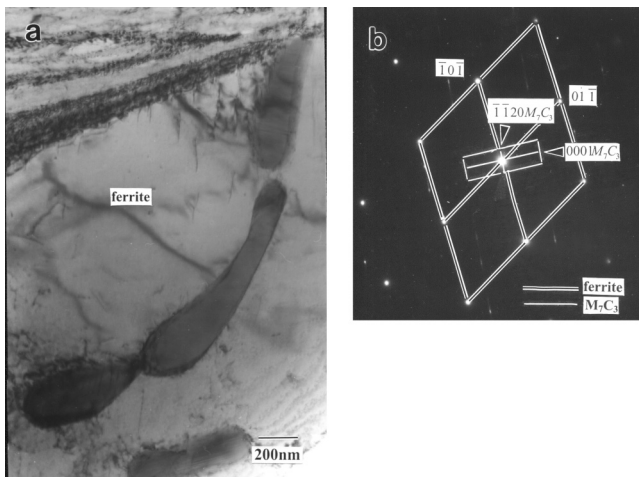
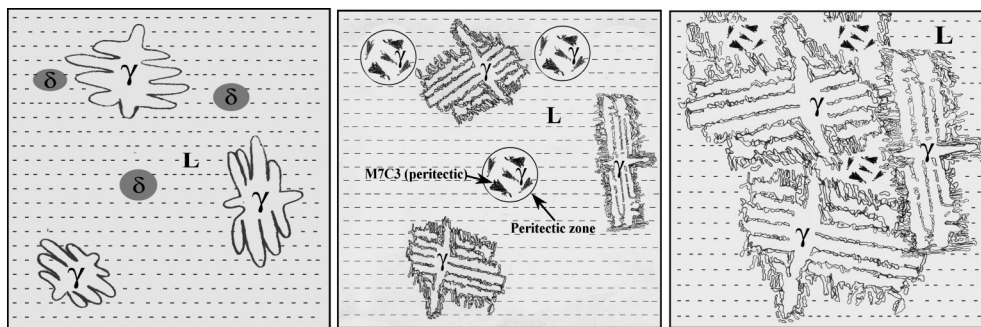


Fig. 9. (a) A bright field TEM micrograph shows carbide particles within the ferrite matrix in iron A. (b) The corresponding selected area diffraction pattern of the M_7C_3 carbide and the ferrite matrix. The angle between $(\bar{1}\bar{1}20)M_7C_3$ plane and $(10\bar{1})$ ferrite plane is about 5 degrees.



(a) Formation of austenite dendrites and δ -ferrite in the melt. The austenite dendrites could nucleate by peritectic reaction or form directly from the melt. (b) Peritectic reaction, $L + \delta \rightarrow M_7C_3$ (peritectic) + γ , started with growth of austenite dendrite and the eutectic constituents continued into the remaining liquid nearby. (c) Growth of primary austenite dendrite was faster than that of the peritectic zone, finally both zones were impinged.

Fig. 10. Schematic drawings show the formation of austenite dendrites and peritectic zones during solidification (a-c).

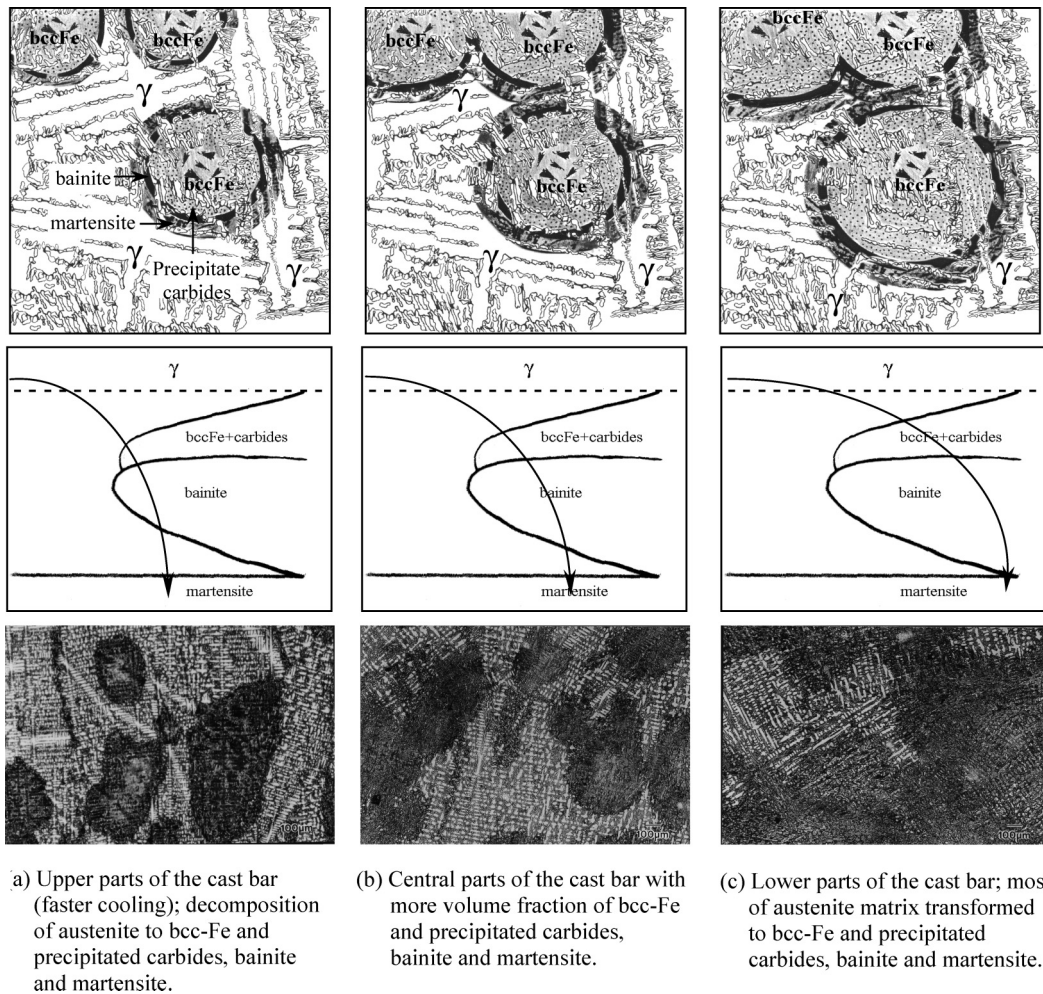


Fig. 11. Transformation of the dendritic austenite to bcc-Fe and precipitated carbides, bainite and martensite, compared between the upper, central and lower parts of the cast bar with different cooling rates (a–c).

cases, if the composition lies close to the P_1U_1 peritectic lie, the peritectic reaction at U_1 may be bypassed in small cast sections due to the faster cooling rate. Hence, in small wear coupons ($15 \times 30 \times 55$ mm in size) cast in Alloy B, no peritectic M_7C_3 was observed in the microstructure. In Alloy B, the cooling rate was also fast enough to prevent any transformation of the primary austenite to ferrite and carbides during cooling in the solid state. For the test bars (25 mm diameter and 300 mm long) cast in Alloy A, the cooling rate was not fast enough to suppress the formation of peritectic M_7C_3 which was seen in all positions in the bar. However, in the top part of the bar, the cooling rate was fast enough to retain a considerable amount of austenite. In the central and lower parts of the bar, much of the austenite transformed to ferrite and carbides. In both alloys, the austenite is expected to form by the $L + \delta \rightarrow \gamma$ peritectic reaction. However, no evidence of this reaction was seen in the microstructures, so it is assumed that, due to non-equilibrium effects, austenite dendrites could nucleate directly from the melt. Further research is needed to understand the exact nature of the solidification sequence in Cr irons with this type of composition.

With regards to wear performance, no work has yet been done on wear testing of this type of structure. However, it is expected that it would give inferior performance when compared to fully austenitic material, particularly if the

wear part is to be used in the as-cast condition. The outer regions containing ferrite and carbides only have a microhardness of around 390 Hv and the smaller core areas containing peritectic M_7C_3 and ferrite have a microhardness of around 350 Hv. These levels are lower than the microhardness of austenite regions (520 Hv). Furthermore, ferrite does not work harden significantly during wear service whereas, under high stress abrasion conditions, austenite can work harden up to 800 Hv.^{15,16} Less differences are expected if the iron is heat treated since previous work has indicated that Alloy A could be successfully hardened by thermal treatment to hardness levels up to 770 Hv.¹⁹ In either case, the peritectic M_7C_3 is finer than the eutectic M_7C_3 carbide, so it should not have damaging effect on toughness or wear performance.

The practical significance of these structural observations is that if 30% Cr irons are to be used in the as-cast condition for abrasion resisting applications, then it is advisable that foundries maintain a minimum C content of 2.5 wt% to ensure that primary ferrite is avoided and that the as-cast matrix is essentially austenitic.

Acknowledgements

The authors would like to thank the Electron Microscopy Research and Service Center (EMRSC), Faculty of Science, Chiang Mai University for provision of electron mi-

croscopy facilities. The work was supported by The Thailand Research Fund (TRF) and by the National Metals and Materials Technology Center (MTEC).

REFERENCES

- 1) C. P. Tabrett and I. R. Sare: *Wear*, **203–204** (1997), 206.
- 2) H. N. Liu, M. Sakamoto, M. Nomura and K. Ogi: *Wear*, **250** (2001), 71.
- 3) J. T. H. Pearce: *Br. Foundryman*, **78** (1985), 13.
- 4) K. A. Kibble and J. T. H. Pearce: *Cast Met.*, **6** (1993), 9.
- 5) J. T. H. Pearce: *Foundryman*, **95** (2002), 156.
- 6) R. W. Durman: *Int. J. Miner. Process.*, **22** (1988), 381.
- 7) D. W. J. Elwell and G. M. Higginson: *World Pumps*, **266** (1988), 209.
- 8) J. T. H. Pearce and D. W. L. Elwell: *J. Mater. Sci. Lett.*, **5** (1986), 1063.
- 9) K. Peev, M. Radulovic and M. Fiset: *J. Mater. Sci. Lett.*, **13** (1994), 112.
- 10) C. P. Tabrett, I. R. Sare and M. R. Ghomashchi: *Int. Mater. Rev.*, **41** (1996), 59.
- 11) P. Dupin, J. Saverna and J. M. Schissler: *AFS Trans.*, **154** (1982), 711.
- 12) G. L. F. Powell and G. Laird: *J. Mater. Sci.*, **27** (1992), 29.
- 13) G. Laird, R. Gundlach and K. Rohrig: *Abrasion-Resistant Cast Iron Handbook*, American Foundry Society, Illinois, (2000), 7.
- 14) J. W. Boyes: *Iron Steel*, **39** (1966), 102.
- 15) J. T. H. Pearce: *AFS Trans*, **126** (1984), 599.
- 16) J. T. H. Pearce: *Wear*, **89** (1983), 333.
- 17) R. S. Jackson: *JISI*, **208** (1970), 163.
- 18) W. R. Thorpe and B. Chicco: *Metall. Trans. A*, **16A** (1985), 1541.
- 19) A. Wiengmoon, T. Chairuangsi and J. T. H. Pearce: *ISIJ Int.*, **44** (2004), 396.
- 20) J. T. H. Pearce: Ph.D Thesis, University of Aston, UK, (1982).
- 21) B. Chicco and W. R. Thorpe: *Cast Met.*, **5** (1993), 203.
- 22) B. K. Arnold and I. R. Sare: *Foundryman*, **82** (1989), 71.
- 23) G. V. Raynor and V. G. Rivlin: *Phase Equilibria in Iron Ternary Alloys*, The Institute of Metals, London, (1988), 143.